12th International Conference on Fracture Mechanics of Concrete and Concrete Structures
FraMCoS-12
B.L.A. Pichler, Ch. Hellmich, P. Preinstorfer (Eds)

https://doi.org/10.21012/FC12.1156
MS13-2:3

ON FPZ FOR MIXED MODE I-II FRACTURE IN CONCRETE AFTER SUSTAINED LOADING USING DIC TECHNIQUE

MAOMAO YANG[1], WEI DONG[1*], WENYAN YUAN[1] AND BINSHENG ZHANG[2]

1 State Key Laboratory of Coastal and Offshore Engineering, Dalian University of Technology
Linggong Road 2, Dalian, 116024, China.
e-mail: maomao1996@mail.dlut.edu.cn.
e-mail: dongwei@dlut.edu.cn (*Corresponding author)
e-mail: yuanwenyan@dlut.edu.cn
2 Department of Civil Engineering and Environmental Management, Glasgow Caledonian University,
Cowcaddens Road, Glasgow, G4 0BA, Scotland, United Kingdom.
e-mail: Ben.Zhang@gcu.ac.uk

Key words: Mixed Mode I-II Fracture, Sustained Loading, Fracture Process Zone, DIC Technique

Abstract: This paper investigates the fracture process zone (FPZ) of mixed mode I-II fracture in concrete after sustained loading, employing the digital image correlation (DIC) technique. Concrete specimens were subjected to sustained three-point bending (TPB) and four-point shearing (FPS) loading for 90 days, with the sustained load level at 80% of the initial cracking load. Afterward, the specimens were unloaded and tested under static loading until failure. The DIC technique was employed to monitor the fracture process of concrete beams after sustained loading. The crack mouth opening displacements obtained from the DIC technique were consistent with those measured using clip gauges, validating the accuracy of the DIC technique. The crack opening displacement field derived from DIC technique was used to determine the size and shape of the FPZ. The lengths of FPZ (l_{FPZ}) for all specimens were measured at peak load. The results indicated that as the ratio of mode II to mode I stress intensity factor (K_{II}/K_I) increased, the l_{FPZ} increased. The l_{FPZ} increase in became more pronounced with higher K_{II}/K_I ratios at peak load. The l_{FPZ} of creep specimens were shorter than those of aging specimens. The increase in l_{FPZ} for creep specimens was less than that for aging specimens. The findings indicated that that the crack propagation resistance improved with a higher mode II component in mixed mode I-II fracture. Additionally, the brittleness of the concrete increased after sustained loading.

1 INTRODUCTION

Concrete gravity dams play a crucial role in flood control, environmental protection, and power generation. However, factors such as construction methods, maintenance conditions, and hydrostatic pressure can result in cracks over time. Due to the random orientation of inherent flaws and discontinuities in concrete, combined with the complexity of loading

systems, cracks in these dams typically experience mixed-mode loading rather than pure mode I. The mixed-mode crack propagation can significantly reduce the dam's load-bearing capacity and increase the risk of structural failure.

As the cracks propagate, a significant nonlinear region develops at the crack tip [1], similar to the plastic zone at the crack tip in metal materials. Unlike ideal brittle materials, crack initiation in quasi-brittle materials does not signify the onset of instability. Instead, it is followed by a stable crack propagation phase. The micro-crack zone and propagation zone at the crack tip are collectively termed the fracture process zone (FPZ). The formation mechanism of FPZ is complex and involves phenomena such as micro-cracking, crack deflection, crack bridging, crack-tip blunting, and crack branching. The FPZ has both degradation and shielding effects on crack propagation, which can reduce the material's strength and stiffness, thereby limiting crack growth. Therefore, it is essential to explore the FPZ for investigating the fracture mechanism of concrete.

For mixed mode I-II fracture in concrete, crack propagation often deviates from the original crack face. To investigate the FPZ, many experimental techniques have been used to monitor the crack propagation process of mixed mode I-II fracture in concrete, such as the acoustic technique, X-rays technique [2], moiré interferometry [2], and optical micros copy [3]. Among these techniques, the digital image correlation (DIC) technique provides a more detailed and accurate visualization of the specimen deformation [4]. Currently, the DIC technology is widely applied in various conditions, such as dynamic cracks of steel fiber-reinforced concrete [5], crack propagation of rock-concrete [4], mixed mode I-II fatigue crack propagation of concrete [6]. Therefore, in this study, the DIC technique was employed to monitor the crack propagation process of mixed mode I-II fracture in concrete. The FPZ can be defined using the stress field [7], displacement field [8], and displacement asymptote matching procedures [9] derived from the DIC technique.

In this paper, three-point bending and four-point shearing loading creep tests and static tests of concrete beams are carried out. The development of cracks after sustained loading is quantitatively analyzed using DIC technique to better understand the FPZ.

2 EXPERIMENTAL PROGRAM

2.1 Specimen preparations

The dimensions of the concrete beams were chosen to be length × width × height =500 × 100 × 100 mm. Concrete with a mix ratio of cement: water: sand: aggregate of 1.00: 0.60: 2.01: 3.68 was used to cast the specimens and the maximum size of the coarse aggregate size was 10 mm. All specimens were naturally aged in the laboratory for 90 days. Prior to testing, a 2 mm wide crack was created on the concrete beams.

The three-point bending (TPB) and four-point shearing (FPS) loading creep and static tests were conducted on the concrete beams. In the TPB loading tests, both the pre-crack and the loading point were positioned along the centerline of the beam cross-section. In the FPS loading tests, the distance from the pre-crack to the centroid of the beam section (C_1) was set at 0 mm and 10 mm, which varied to cover a range of the mode II to mode I stress intensity factor ratios. The distance from two loading points to the centroid of the beam section were set to 200mm and 33mm, respectively, resulting in a load distribution of 33/233P and 200/233P. The pre-crack length (a_0) is 30mm. The geometries of concrete

beams and test layouts are depicted in Figure 1.

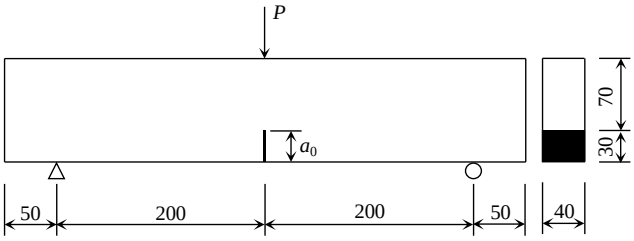

(a) TPB loading beam

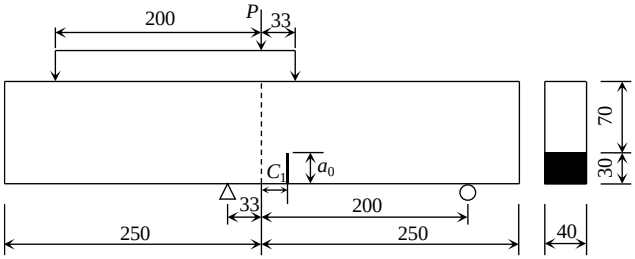

(b) FPS loading beam

Figure 1: Geometries and test layouts of concrete beams.

2.2 Digital image correlation

The digital image correlation (DIC) technique is an optical, non-contact measurement technique, which is employed to analyze the displacement field and strain field on a specimen surface. By comparing images of the specimen before and after deformation, the deformation of a specimen caused by the applied load can be evaluated using the DIC technique.

In the application of DIC technique, the first step is to prepare the specimen's surface with a random speckle pattern that accurately reflects deformation information. During the experimental process, surface images of the specimen are captured before and after loading using a digital camera, and these images are stored on a computer, as shown in Figure 2. The digital camera converts the captured speckle patterns into discrete grayscale intensity values for each pixel. After image acquisition, a grid is applied to the region of interest in the undeformed image. Each sub-region is treated as a rigid motion unit, commonly referred to as a subset or small element in the DIC technique. For each subset, a specific search strategy is employed, and calculations are performed using a pre-defined correlation function. The region in the deformed image that maximizes the cross-correlation coefficient with the corresponding subset in the undeformed image is identified as the deformed position of the subset, enabling the determination of its displacement. The normalized cross-correlation function is one of the commonly used correlation functions [10,11], and its calculation is given by Eq. (1). Initial and deformed patterns are illustrated in Figure 3.

$$G(u,v)=\frac{\sum_{x,y}\left[f(x,y)-\bar{f}\right]\left[g(x+u,y+v)-\bar{g}\right]}{\sqrt{\sum_{x,y}\left[f(x,y)-\bar{f}\right]^2\sum_{x,y}\left[g(x+u,y+v)-\bar{g}\right]^2}} \quad (1)$$

In which, $f(x, y)$ and $\bar{f}$ represent the gray value in the sub-region in the reference image and the mean value; $g(x+u, y+v)$ and $\bar{g}$ represent the gray value in the corresponding sub-region in the deformed image and the mean value; (u, v) represents the displacement of the sub-region in the horizontal and vertical directions.

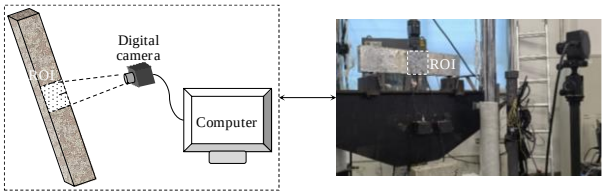

Figure 2: The testing system of DIC technique.

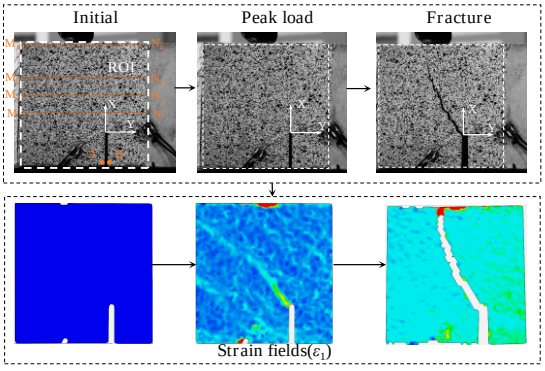

Figure 3: Initial and deformed patterns.

2.3 Experimental setup

To calibrate the applied load in the creep tests, the concrete beams were initially tested under TPB and FPS loading in a 250-kN closed-loop servo-mechanical testing machine (MTS) at a displacement rate of 0.024 mm/min. The displacement at the loading point (δ) was measured using a linear variable displacement transducer (LVDT), while the crack mouth opening displacement (*CMOD*) and crack mouth sliding displacement (*CMSD*) were measured using clip gauges. Additionally, to determine the initial cracking load (P_{ini}), four strain gauges were symmetrically placed on both sides of the specimen, 5 mm away from the tip of the pre-crack in the ligament. It should be noted that in the FPS loading beams, the strain gauges were aligned in the direction of the maximum principal tensile strain [12]. Before crack initiation, the strain at the crack tip increased gradually with the applied load, leading to the accumulation of the energy. When a new crack occurs, the stored energy is released, the strain reaches its maximum and initiates crack propagation. This resulted in a distinct retraction point on the load-strain curve, with the load corresponding to this point being referred to as the initial cracking load (P_{ini}) [13].

Eighteen concrete beams were then prepared and divided into six groups, with each group consisting of three beams. The sustained load (P_{sus}) for creep tests was set at 80% of the initial cracking loading ($0.8P_{ini}$). Based on the sustained loading level and the value of C_1, the creep specimens were labeled as C-TPB-$0.8P_{ini}$, C-FPS-$0.8P_{ini}$-10 and C-FPS-$0.8P_{ini}$-0. The aging specimens, which were not subjected to sustained loading, were labeled as A-TPB, A-FPS-10 and A-FPS-0. Here, "C" and "A" represent creep and aging specimens, respectively; $0.8P_{ini}$ represents 80% of the initial cracking load; 0 and 10 represent the distances from the pre-crack to the centroid of the beam section.

The creep tests were conducted in a controlled environment with a temperature of 20 ± 2°C and 50% relative humidity. The creep specimens were loaded in steel frames for the TPB and FPS loading creep tests. A bolt was fixed vertically to the steel frame, and the designed load (P_{sus}) could be applied on the creep specimen by rotating the bolt. A load cell attached to the bolt was connected to a data collection system with a digital display to record the load in real-time, ensuring that the specified load value was maintained. If the applied load dropped by more than 2%P_{sus}, it was adjusted back to the specified value. Two mechanical dial gauges were used to measure the displacement at the loading point and the crack mouth opening displacement. Additionally, the aging specimens were also placed in the same room. The setup for the creep tests is depicted in Figure 4.

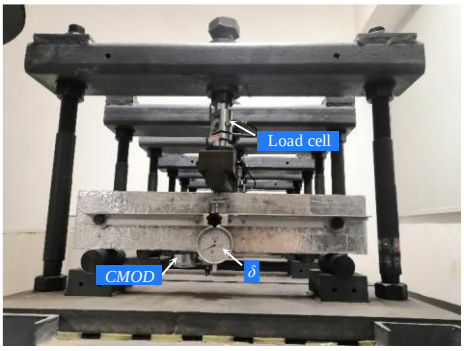

(a) TPB loading

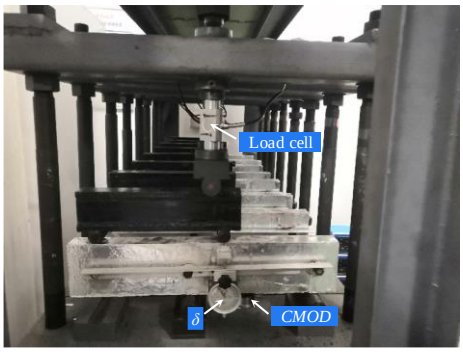

(b) FPS loading

Figure 4: The setups of the creep tests.

After the creep tests, the creep specimens were unloaded from the steel frames, and then the creep specimens and aging specimens were moved to the MTS testing machine for the TPB and FPS loading static tests. In the static tests, a digital camera with a resolution of 2746×3584 pixels were positioned in front of the concrete beams, with its lens parallel to the lateral surface of the specimen. The testing system is illustrated in Figure 2. The experimental results are summarized in Table 1, where P_{ini}, P_{max}, K_{II} and K_I represent the initial cracking load, peak load, mode II and mode I stress intensity factors at crack initiation, respectively. The mode II and mode I stress intensity factors can were determined using the displacement extrapolation method [14]. The fundamental mechanical properties of concrete were determined according the Chinese standard (see GB/T 50081-2002-Standard for test method of mechanical properties on ordinary concrete). The compressive strength was measured by compression testing on the 150 mm cube specimens under the force-control mode at a loading rate of 10 kN/s, the tensile strength was measured by splitting tension testing on the 150 mm cube specimens under the force-control mode at a loading rate of 2 kN/s, and the elastic modulus and Poisson's ratio were measured from the compression testing on the prism specimens of 300 mm × 150 mm × 150 mm under the force-control mode at a loading rate of 10 kN/s. Therefore, the fundamental mechanical properties of the concrete at the ages of 90 days are determined. The measured properties were as follows: tensile strength (f_t), Young's modulus and Poisson's ratio are 3.76MPa, 32.43GPa and 0.22, respectively.

Table 1: The experimental results of concrete specimens

Specimen	K_{II}/K_I	P_{ini} /kN	P_{max} /kN	l_{FPZ} /mm
A-TPB-1	0	1.60	2.04	13.34
A-TPB-2		1.63	1.98	9.7
A-TPB-3		1.58	2.16	10.12
Mean		1.60	2.06	11.05
C-TPB-0.8P_{ini}-1		1.93	2.07	8.76
C-TPB-0.8P_{ini}-2		1.93	2.10	11.78
C-TPB-0.8P_{ini}-3		1.90	2.13	8.13
Mean		1.92	2.10	9.55
A-FPS-10-1	1.12	9.09	12.57	16.74
A-FPS-10-2		9.02	12.73	22.7
A-FPS-10-3		9.70	12.72	20.71
Mean		9.27	12.67	20.05
C-FPS-0.8P_{ini}-10-1		10.25	12.29	9.05
C-FPS-0.8P_{ini}-10-2		10.40	11.66	16.55
C-FPS-0.8P_{ini}-10-3		10.30	11.81	15.05
Mean		10.32	11.92	13.55
A-FPS-0-1	13.40	10.06	14.10	20.01
A-FPS-0-2		9.68	13.60	22.2
A-FPS-0-3		10.74	15.07	23.48
Mean		10.16	14.26	21.9
C-FPS-0.8P_{ini}-0-1		10.98	14.34	20.96
C-FPS-0.8P_{ini}-0-2		11.12	14.19	18.51
C-FPS-0.8P_{ini}-0-3		10.87	14.58	22.58
Mean		10.99	14.37	20.68

3 EXPERIMENTAL RESULTS AND DISCUSSION

3.1. The validity of the DIC technique

To verify the validity of the DIC technique,

crack mouth opening displacements (*CMOD*) were extracted. A distinct region of interest (ROI) was carefully selected on the specimen surface, with the size of the ROI being 80 mm×100 mm, as shown in Figure 3. Points A and B represent the pixels on either side of the crack mouth. The difference in the horizontal displacement (u_x) between two points defines the *CMOD*. Taking one specimen from each group of creep specimens as the example, the load versus crack mouth opening displacement (*P-CMOD*) curves obtained using both the DIC technique and clip gauges are shown in Figure 5. The results from the two methods are in good agreement, validating the DIC technique as reliable for measuring crack opening displacement, crack propagation length and crack propagation path.

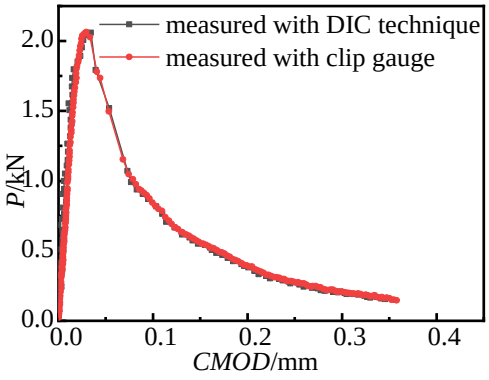

(a) C-TPB-0.8P_{ini}-3

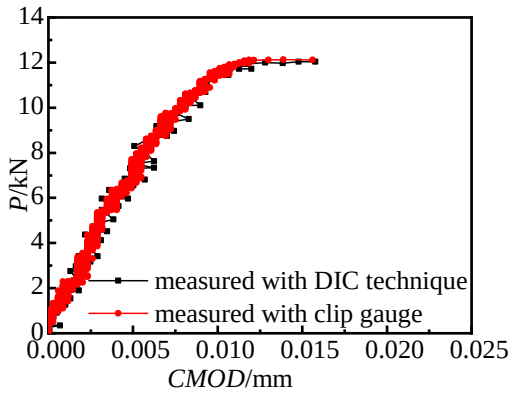

(b) C-FPS-0.8P_{ini}-10-3

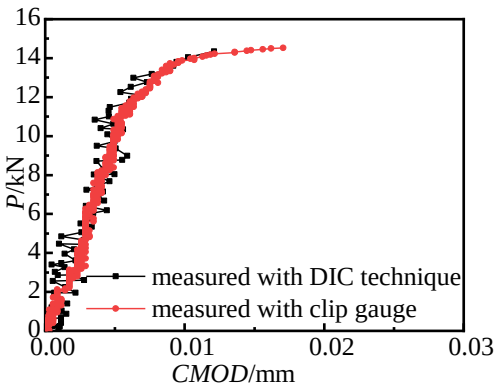

(c) C-FPS-0.8P_{ini}-0-3

Figure 5: The *P-CMOD* curves obtained using both the DIC technique and clip gauges.

3.2. The determination of FPZ

Taking specimen A-FPS-10-1 as an example, the image corresponding to the peak load was selected to illustrate how the FPZ and crack opening displacement (*COD*) and crack sliding displacement (*CSD*) are determined. Firstly, by picking up one out of each seven pixels, computational grid points were selected at intervals of to conduct the deformation analysis in the X (perpendicular to the crack surface) and the Y (parallel to the crack surface) directions. Line MN is positioned just above the pre-crack tip, and Lines M_1N_1, M_2N_2, ..., M_nN_n (n = 194) are parallel to Line MN with an interval of seven pixels, as show in Figure 3. The crack opening displacement (u_x) along the X direction and sliding displacement (v_y) along the Y direction for various loading conditions were calculated using the DIC technique. Here, the points at the boundary of the displacement jump are denoted as Points Q and R on line MN. The *COD* is defined as the difference in u_x between points Q and R, while the *CSD* is defined as the difference in v_y between these points. The distance between the two points represents the crack width. The *COD* and *CSD* along line MN are obtained, from which the crack profile for line MN can be derived. The

same procedure is repeated for lines M_1N_1, M_2N_2, ..., M_nN_n until both displacements became zero, effectively capturing the crack tip. Accordingly, the crack profile is reconstructed.

To determine the FPZ, the critical steps are to locate the crack tip and to determine the length of the FPZ. Currently, there are three methods commonly employed to determine the crack tip. The first method measures the *COD* and *CSD*. The crack tip is defined as the point where both the *COD* and *CSD* are zero [15]. The second method captures the strain field, where the crack tip is identified by the tensile strain corresponding to crack initiation [5]. The third method identifies the crack tip as the point where the displacement contours merge [16]. Due to the discontinuity of the displacement field in the FPZ affecting the derived strain field and the subjectivity involved in determining the merged point, the crack tip was determined by combining the first and second methods. As expected, the *COD* and *CSD* gradually decrease as Line M_nN_n moves away from Line MN. The crack tip was determined to extend to Line M_nN_n where the *COD* and *CSD* are equal to zero. Furthermore, according to the tension-softening constitutive law of the concrete proposed by Dong et al. [4], the critical crack opening displacement (w_0) for concrete beams equals $3.6G_f/f_t$ mm, which equals 0.105mm, where G_f represents the fracture energy, determined using the standardized method suggested by RILEM [17]. When the *COD* along Line MN reaches the w_0, the FPZ is considered fully developed. At this point, the FPZ was identified as the concrete zone extending from Line MN to Line M_nN_n. The crack trajectories and the determined FPZ for specimen A-FPS-10-1 at the peak load are shown in Figure 6, where the left image was taken after fracture and the right image was captured using the DIC technique. The close similarity between the two images confirms the applicability of the DIC technique for determining the FPZ of mixed-mode I-II fracture in concrete.

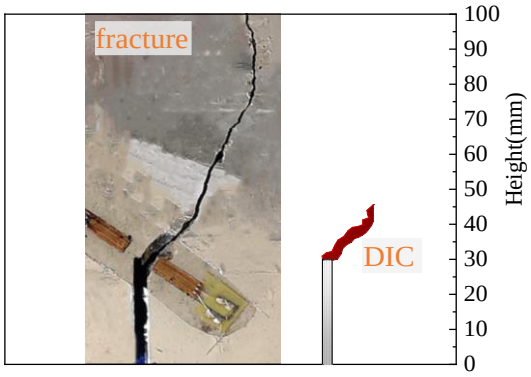

(a) The crack trajectories

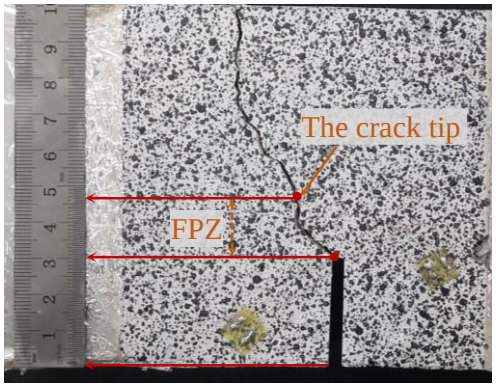

(b) FPZ

Figure 6: The determination of FPZ for specimen A-FPS-10-1.

3.3. The length of FPZ

Taking one specimen from each group of creep specimens as the example, the strain field is shown in the left images of Figure 7. It can be seen that as the load increased, the crack propagated. Simultaneously, the fracture process zone developed, and the length of the FPZ increased. As the crack propagated, the mode II stress intensity factor decreased, causing the crack propagation path to gradually straighten. Using the aforementioned DIC technique, the crack opening displacements (u_x) of both Line MN and Line M_nN_n at the peak load were obtained and depicted in the right images of Figure 7. As shown in Figure 7, the

crack opening displacement between points Q and R along Line MN exhibited a significant magnitude, while the difference in u_x values was less than the critical crack opening displacement. This suggests that the FPZ was not fully developed at the peak load. The crack opening displacement approached zero along Line M_nN_n, indicating that the crack tip was located at this line. Thus, the length of the FPZ (l_{FPZ}) was determined by connecting the midpoint of Line MN to the crack tip, and it was found to be equal to the crack propagation length.

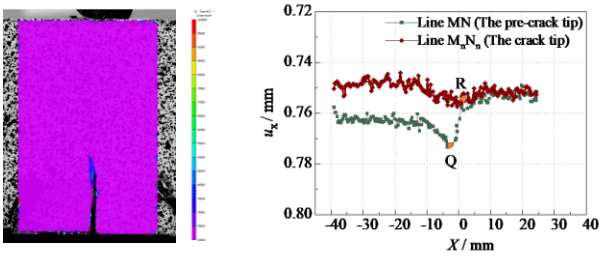

(a) C-TPB-0.8P_{ini}-2

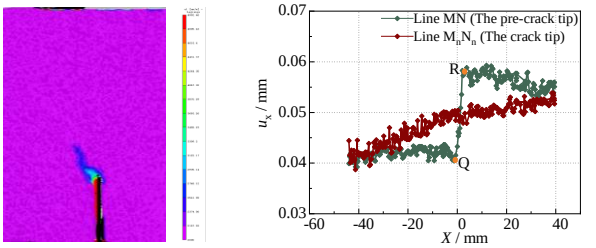

(b) C-FPS-0.8P_{ini}-10-2

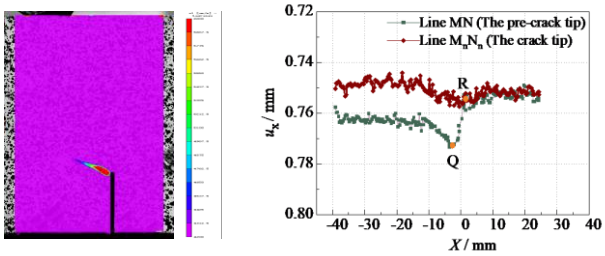

(c) C-FPS-0.8P_{ini}-0-2

Figure 7: The strain fields and crack opening displacements of concrete specimens.

The l_{FPZ} of all concrete specimens at the peak load are illustrated in Figure 8, Figure 9 and Table 1. As shown in Figure 8, as the K_{II}/K_I ratio increased, l_{FPZ} for both aging and creep specimens increased. As the K_{II}/K_I ratio increased, the increments in l_{FPZ} increased. In Figure 8, the l_{FPZ} of the creep specimens were shorter than those of the aging specimens. The increments of l_{FPZ} of creep specimens were less than those of aging specimens. The findings suggest that the crack propagation resistance increased with the increase in the mode II component in mixed mode I-II fracture. Moreover, the brittleness of the concrete increased after sustained loading.

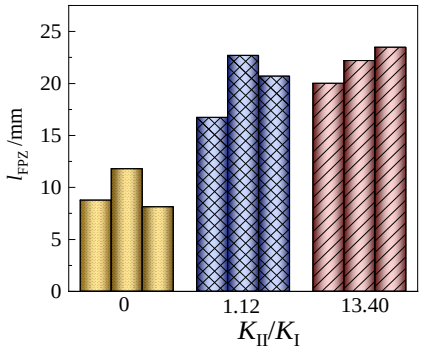

(a) Aging specimens

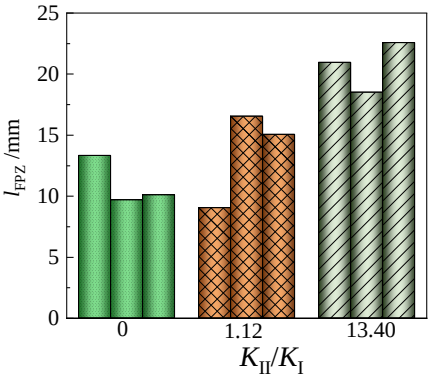

(b) Creep specimens

Figure 8: Comparisons of l_{FPZ} for different ratios of mode II to mode I stress intensity factors.

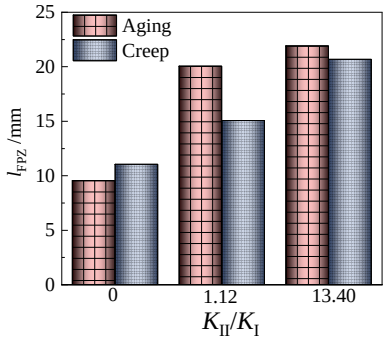

(a) l_{FPZ}

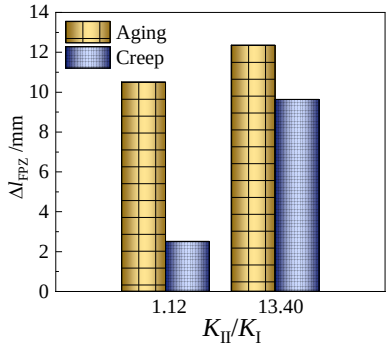

(b) Δl_{FPZ}

Figure 9: Comparisons and increments of l_{FPZ} between aging and creep specimens.

4 CONCLUSIONS

In this paper, the fracture process zone (FPZ) for mixed mode I-II fracture in concrete after sustained loading was investigated through three-point bending and four-point shearing loading tests, combined with the Lagrange strain monitoring results obtained using the DIC technique. The main findings are summarized as follows:

(1) The entire process from initiation to failure of concrete mixed mode I-II fracture can be clearly captured using the DIC technique in the static tests. The crack opening displacement field derived from DIC technique can be utilized to determine the size and shape of the fracture process zone (FPZ) in mixed mode I-II fracture in concrete.

(2) The lengths of FPZ (l_{FPZ}) specimens at peak load were obtained for all concrete using the DIC technique. As the ratio of mode II to mode I stress intensity factors (K_{II}/K_I) increased, the l_{FPZ} for both aging and creep specimens increased. As the K_{II}/K_I increased, the increments in l_{FPZ} increased at the peak load. The l_{FPZ} of creep specimens were shorter than those of aging specimens. The increments of l_{FPZ} for creep specimens were less than those for aging specimens. The findings indicate that the crack propagation resistance increases with the increase in the mode II component of mixed mode I-II fracture. Additionally, the brittleness of the concrete increased after sustained loading.

REFERENCES

[1] Xu, S. and Reinhardt, H.W., 1999. Determination of double-K criterion for crack propagation in quasi-brittle fracture, Part I: Experimental investigation of crack propagation. *Int. J. Fract*. **98**: 111-149.

[2] Otsuka, K. and Date, H., 2000. Fracture process zone in concrete tension specimen. *Eng. Fract. Mech.* 65, **2**:111-131.

[3] Hadjab.S, H., Chabaat, M. and Thimus, J.-Fr., 2007. Use of scanning electron microscope and the non-local isotropic damage model to investigate fracture process zone in notched concrete beams. *Exp. Mech.* 47, **4**: 473-484.

[4] Dong, W., Wu, Z. and Zhou, X. et al., 2017. FPZ evolution of mixed mode fracture in concrete: experimental and numerical. *Eng. Fail. Anal.* **75**: 54-0.

[5] Pan, K., Yu, R.C. and Ruiz, G. et al., 2021. The propagation speed of multiple dynamic cracks in fiber-reinforced cement-based composites measured using DIC. *Cem. Concr. Compos.* **122**: 104140.

[6] Jia, M., Wu, Z. and Yu, R.C. et al., 2022. Experimental and numerical study on mixed mode I-II fatigue crack propagation in concrete. *J. Eng. Mech.* 148, **9**: 04022044.

[7] Dai, Y., Gruber, D. and Harmuth, H., 2017. Observation and quantification of the fracture process zone for two magnesia

refractories with different brittleness. *J. Eur. Ceram. Soc.* 37, **6**: 2521-2529.
[8] Trivedi, N., Singh, R.K. and Chattopadhyay, J., 2015. Investigation on fracture parameters of concrete through optical crack profile and size effect studies. *Eng. Fract. Mech.* **147**: 119-139.
[9] Bhowmik, S. and Ray, S., 2019. An experimental approach for characterization of fracture process zone in concrete. *Eng. Fract. Mech.* **211**: 401-419.
[10] Shah S.G. and Kishen J. M. C., 2011. Fracture properties of concrete-concrete interfaces using digital image correlation. *Exp. Mech*. **51**(3): 303-313.
[11] Soranakom, C. and Mobasher, B., 2008. Correlation of tensile and flexural responses of strain softening and strain hardening cement composites. *Cem. Concr. Compos.* 30, **6**: 465-477.
[12] Yates, J.R., Zanganeh, M. and Tai, Y.H., 2010. Quantifying crack tip displacement fields with DIC. *Eng. Fract. Mech.* 77, **11**: 2063-2076.
[13] Yang, M., Dong, W. and Yuan, W. et al., 2024. Fracture properties of mixed mode I-II cracks in concrete after sustained loading. *Eng. Fract. Mech.* **309**: 110394.
[14] Zhao, X., Dong, W. and Zhang, B. et al., 2023. Fracture properties of rock-concrete interface after fatigue loading. *J. Mater. Civ. Eng.* 35, **4**: 04023033.
[15] Dong, W., Wu, Z. and Zhou, X. et al., 2016. A comparative study on two stress intensity factor-based criteria for prediction of mode-I crack propagation in concrete. *Eng. Fract. Mech.* **158**: 39-58.
[16] Shah, S.G. and Chandra Kishen, J.M., 2011. Fracture properties of concrete-concrete interfaces using digital image correlation. *Exp. Mech.* 51, **3**: 303-313.
[17] Lin, Q., Yuan, H. and Biolzi, L. et al., 2014. Opening and mixed mode fracture processes in a quasi-brittle material via digital imaging. *Eng. Fract. Mech.* **131**: 176-193.
[18] Vandewalle, L., Nemegeer, D. and Balazs, L. et al., 2003. RILEM TC 162-TDF: Test and design methods for steel fibre reinforced concrete' - sigma-epsilon-design method - Final Recommendation. *Mater Struct.* 36, **262**: 560-567.